Contents lists available at ScienceDirect

Arabian Journal of Chemistry

journal homepage: www.ksu.edu.sa

Green synthesis and antibacterial assessment of chitosan/silver nanocomposite conjugated with tobramycin against antibiotic resistant *Pseudomonas aeruginosa*

Shahid Wahab [a,b,1], Haroon Muhammad Ali [c], Maham Khan [c], Tariq Khan [c], Chandran Krishnaraj [a,b,1], Soon-Il Yun [a,b,*]

[a] Department of Food Science and Technology, Jeonbuk National University, Republic of Korea
[b] Department of Agricultural Convergence Technology, Jeonbuk National University, Republic of Korea
[c] Department of Biotechnology, University of Malakand, Chakdara, Dir Lower, Pakistan

ARTICLE INFO

Keywords:
Silver nanoparticles
Chitosan nanoparticles
Silver/chitosan nanocomposite
Silver/chitosan/tobramycin conjugation
Antibiotic resistance

ABSTRACT

In this study, we employed aqueous ginger extract as an eco-friendly approach for the synthesis of chitosan nanoparticles (CsNPs), silver nanoparticles (AgNPs), and chitosan/silver nanocomposites (Cs/AgNCs). Using spectroscopic and microscopic techniques, we thoroughly characterized the physicochemical properties of these nanomaterials, confirming their desirable attributes. The AgNPs displayed a spherical morphology with an average diameter of 19 nm, while the Cs/AgNCs exhibited a size of approximately 28 nm. To assess their antibacterial efficacy, we investigated the activity of both AgNPs and Cs/AgNCs against Gram-negative pathogenic bacteria. Remarkably, these nanomaterials demonstrated significant antibacterial properties. To further enhance their antibacterial capabilities, we conjugated the nanocomposite with tobramycin using Sulfo NHS and EDC, resulting in a four-fold increase in antibacterial activity compared to tobramycin alone. Moreover, we explored the ability of AgNPs, CsNPs, Cs/AgNCs, and Cs/AgNCs/tobramycin (Cs/AgNCs/tbn) to degrade DNA and generate reactive oxygen species (ROS) in the presence of *Pseudomonas aeruginosa*. Encouraging results were obtained, highlighting their potential applications in antimicrobial strategies. Furthermore, we conducted a comprehensive toxicity assessment of AgNPs, CsNPs, Cs/AgNCs, and Cs/AgNCs/tob using zebrafish embryos. The findings revealed low to moderate levels of toxicity for these nanomaterials, with Cs/AgNCs/tbn demonstrating no observable toxic effects. Our study demonstrates the immense potential of utilizing aqueous ginger extract as a green synthesis method to produce AgNPs and Cs/AgNCs with robust antibacterial properties and minimal toxicity. These findings pave the way for the development of innovative nanomaterials for various biomedical applications.

1. Introduction

Since the rate of developing antibiotic resistance is increased due to excessive misuse of antibiotics, a great risk of the emergence of new infectious diseases caused by resistant pathogens is posed to human health (Shao et al., 2021). *Pseudomonas aeruginosa* is the one of disreputable pathogenic bacteria that can escape the effects of antibiotics and has developed resistance to several currently available antimicrobial regimes. It is part of ESKAPE that refers to a group of multi-drug resistant bacteria including *Enterococcus faecium, Staphylococcus aureus, Klebsiella pneumoniae, Acinetobacter baumannii, Pseudomonas aeruginosa*, and *Enterobacter* sp. *P. aeruginosa*, a Gram-negative bacterium of this group, develops as a notable pathogen causing a threat to human health worldwide (Armijo et al., 2020). It causes nosocomial infections and lethal infections in immune-compromised individuals such as patients with cancer, AIDS, serious burns, and post-surgery. In 2017, the World Health Organization listed *P. aeruginosa* as the preferred agent for the research and development of novel antibiotics (Thi et al., 2020). This

Peer review under responsibility of King Saud University.
* Corresponding author.
E-mail address: siyun@jbnu.ac.kr (S.-I. Yun).
[1] These authors equally contributed.

https://doi.org/10.1016/j.arabjc.2023.105458
Received 7 June 2023; Accepted 13 November 2023
Available online 14 November 2023

pathogen utilizes all three forms of resistance mechanisms i.e., intrinsic (lower cell wall permeability, activate efflux pump, and produce antibiotic degrading enzymes), acquired (achieved through horizontal gene transfer), and adaptive (formation of resistant biofilms) to result in a recalcitrant strain. The development of drugs that can simultaneously target multiple sites and/or mechanisms of resistant pathogenic bacteria is a major challenge in the public health sector (Pang et al., 2019).

Nanoparticles such as AgNPs have gained enormous attention as antimicrobial agents because of their unique properties such as small in their size and large surface area to volume ratio. Due to the size of the particles lying on the nanoscale, they can target multiple sites of action. AgNPs can disrupt the outer membrane of bacteria, releasing silver ions that cause oxidative damage affecting the positioning of nucleotides that lead to the disruption of DNA. AgNPs are effective against both Gram-positive and Gram-negative bacteria (Khan et al., 2023). AgNPs can be synthesized through biological means using plant extracts which is the safest and most efficient method for the synthesis of nanoparticles (Wahab et al., 2021). The present study involved the synthesis of AgNPs using ginger (*Zingiber officinale*) extract. Ginger is native to tropical Asia. The rhizomes of the plant are used as spices worldwide with a strong fragrance. Usually, it is used in various products such as medicines including those against Coronavirus diseases. Due to the existence of vital phytochemicals like flavonoids, flavones, anthocyanin, coumarin, lignans, and catechins, it possesses both antibacterial and antioxidant qualities (Kumar et al., 2014). Moreover, it serves as an abundant reservoir of active compounds, notably bioactive phenols such as gingerols, shogaols, and zingerones (Wang et al., 2020). These phytochemicals allow ginger to be used for stomach ache and cough, and to reduce chemotherapy-induced nausea in cancer patients (Hu et al., 2022). Thus, the literature indicates the use of ginger extract as a potential source for the effective synthesis of AgNPs.

Recently, metal nanoparticles have been immobilized on polymers, allowing them to be integrated into polymers, a hybrid is formed that prevents the particles from aggregation. These polymers like chitosan act as a matrix that controls the nanoparticles' growth and stabilization (Wang et al., 2015). In addition, the immobilization of AgNPs on chitosan could prevent the diffusion of AgNPs into the environment and biosphere where they can accumulate and cause side effects, to reduce the risk related to the use of antimicrobials containing AgNPs is one of the main considerations (Mori et al., 2013). AgNPs loaded on chitosan composites (Cs/AgNCs) were reported to possess robust antibacterial activities against Gram-positive and Gram-negative bacteria. Both chitosan and AgNPs individually have been evaluated for their remarkable antimicrobial activity. Combining the effect of these two components could result in the formation of an agent with diverse antimicrobial properties (Yang et al., 2016). Moreover, conjugating and joining antimicrobial nanoparticles, such as AgNPs with antibiotics have been reported as assuring antibacterial agents (Jelinkova et al., 2019). So far tobramycin, an aminoglycoside, is the most active drug against *P. aeruginosa* which has been recommended by several studies to be used in conjunction with nanomaterials to further enhance its efficiency (Armijo et al., 2020). AgNPs can act as a drug-delivery tool and are reported to improve the pharmacokinetics of antibiotics. The conjugate of tobramycin-AgNPs may have the following advantages: targeting multiple sites of bacteria, decreasing the number of emerging resistant pathogens, facilitating the self-assembly of antimicrobials in nanostructures for effective delivery, prolonging drug circulation and stability in the body, reducing the frequency and quantity of doses, thereby lowering toxicity (Ribeiro et al., 2022). Previous research reported the synthesis of antibiotic-nanomaterial conjugates by using chemicals such as 3-ethyldimethylaminopropyl carbodiimide (EDC) and N-hydroxy succinimide (NHS) (Tyagi et al., 2020).

In this study, we compare the effect of AgNPs synthesized from ginger extract, CsNPs, Cs/AgNCs, and Cs/AgNCs/tbn against *Pseudomonas aeruginosa*. This study aims to filter out the best antibacterial agent to be used in infections caused by *P. aeruginosa* with minimum or no toxicity.

2. Materials and methods

2.1. Materials

The *Zingiber officinale* rhizome (ginger) was purchased from a local shop in Jeonju, South Korea. Silver nitrate ($AgNO_3$), chitosan, tobramycin, 2′,7′-Dichlorodihydrofluorescein diacetate (H2DCFDA), 3-ethyldimethylaminopropyl carbodiimide (EDC), N-Hydroxy succinimide (NHS), 3-(4,5-dimethylthiazol-2-yl)-2,5-diphenyl-2H-tetrazolium bromide (MTT), sodium hydroxide (NaOH), acetic acid, tris, Triton X-100, and sodium tripolyphosphate (STPP) were purchased from Sigma Aldrich. Nutrient agar and broth were obtained from Difco. The bacterial strain *Pseudomonas aeruginosa* was obtained from the Korea Collection for Type Cultures (KTCC).

2.2. Synthesis of AgNPs

Fresh ginger was obtained from a local market in Jeonju City, South Korea, and was cleaned with deionized water ($D{\cdot}H_2O$). The ginger was sliced and dried in an oven. Subsequently, 5 g of the dried ginger were mixed with 50 mL of $D{\cdot}H_2O$ and boiled at 70 °C for 3 h. After cooling down, the resulting extract was filtered using Whatman filter paper, followed by sonication for 10 min at 40 kHz. To prepare the $AgNO_3$ solution, 8.5 mg (1 mM) of $AgNO_3$ was dissolved in 25 mL of $D{\cdot}H_2O$, and this solution was then mixed with 25 mL of the ginger extract. The mixture was heated at 70 – 80 °C. After 30 min, the reaction mixture changed color from transparent to sparkling yellow and subsequently to sparkling brown after 1 h, indicating the synthesis of AgNPs. The formation of AgNPs was confirmed by monitoring the UV–Vis absorption spectrophotometric (Hewlett Packard (HP 8453) throughout the reaction.

2.2.1. Synthesis of CsNPs

The CsNPs were prepared by optimizing the previously reported protocol of Krishnaraj et al., (2022). Briefly, a chitosan solution was prepared by slowly dissolving 40 mg of chitosan in 100 mL of 1 % acetic acid. The pH of the solution was carefully adjusted to > 6 using 1 M NaOH. Subsequently, 25 mL of the ginger extract was introduced into the chitosan solution, and the two constituents were carefully mixed using a magnetic stirrer. In this stirring, 8 mL of 0.1 % STPP was gradually added dropwise through a syringe needle, all while the stirring process continued for 45 min. The resultant mixture was stored at room temperature for 24 h. The formation of CsNPs was validated through UV–Vis spectrophotometric analysis (Hewlett Packard (HP 8453).

2.2.2. Synthesis of Cs/AgNCs

To synthesize the Cs/AgNCs, a solution of 100 mL of AgNPs was synthesized by following the earlier used protocol mentioned in the previous section (*2.2*). To this, a chitosan solution was prepared by slowly dissolving 40 mg of chitosan in 100 mL of 1 % acetic acid. The pH of the solution was carefully adjusted to > 6 using 1 M NaOH**.** Subsequently, a ginger extract of 25 mL was added to the mixture and thoroughly stirred via a magnetic stirrer. Using a syringe needle, 8 mL of a 0.1 % solution of STPP was carefully added drop by drop into the test solution. The resulting mixture was stirred for 45 min, after which it was left undisturbed at room temperature for 24 h. Regular sampling was conducted for analysis using a UV–Vis spectrophotometer (Hewlett Packard (HP 8453).

2.2.3. Synthesis of Cs/AgNCs/tbn

To conjugate Cs/AgNCs with tobramycin, EDC and Sulfo-NHS were used. Using Sulfo-NHS, carboxyl groups are turned into an amine-reactive ester, facilitating cross-linking or bioconjugation. It is a charged version of NHS (N-hydroxy succinimide) and can be used to

modify carbodiimide crosslinking reactions. A carboxylate (–COOH) present in the polymer molecule is activated so that it can be conjugated with the primary amine (–NH_2) found in tobramycin (Armijo et al., 2020). Initially, 10 mg of tobramycin was dissolved in a mixture of 20 mL of DMSO and D·H_2O in a 1:1 ratio. The solution was then sonicated for 20 min at 50 kHz. Following this, 5 mg of EDC was added to the solution while continuously stirring. Subsequently, 5 mg of NHS was added, and the pH was adjusted to 6. The solution was kept in the dark for 3 – 4 h to allow the conjugation reaction to occur (forming "solution 1″). Next, 20 mg of Cs/AgNCs was suspended in 5 mL of a 1:1 mixture of DMSO and D·H_2O This suspension was added to "solution 1," and the pH was adjusted to 8. The mixture underwent stirring for 12 h. Once the specified time elapsed, the solution was centrifuged at a speed of 7000 rpm for 12 min. The supernatant was removed, and the resulting pellet was washed three times using DMSO followed by ethanol. Later, the remaining pellet was dried at a temperature of 65 °C for 3 h to obtain the conjugate nanoparticles. The characterization of the conjugate nanoparticles was performed using FTIR. Finally, the nanoparticles were stored at 4 °C for further usage (Tyagi et al., 2020). Fig. 1. Describes the formation of Cs/AgNCs/tbn.

2.3. Characterization of nanomaterials

The plant extract, CsNPs, AgNPs, and Cs/AgNCs were dissolved in D·H_2O and characterized by scanning the nanoparticle solutions using a UV–Visible spectrophotometer in the range of 250 – 600 nm (Hewlett Packard (HP 8453). Additionally, an extra 15 min of centrifugation at 14,000 rpm was performed on the synthesized mixtures. The resulting pellets were collected, cleaned, freeze-dried, and stored. For transmission electron microscopic (TEM) examination of the sizes and shapes of the nanoparticles, the nanoparticles were mixed with 1 mL of D·H_2O Then, 25 µL aliquots of CsNPs, AgNPs and Cs/AgNCs were placed on TEM grids, air-dried, and imaged using a Hitachi H-7650 electron microscope with an accelerating voltage of 80 to 100 kV. FE-SEM (Field Emission Scanning Electron Microscopy) and EDS (Energy-Dispersive X-ray Spectroscopy) analyses were carried out on freeze-dried powder. The samples were coated with carbon tape and then platinum-coated before analysis, using a Carl Zeiss SUPRA40VP microscope. Structural analysis of CsNPs, AgNPs, and Cs/AgNCs was performed using HR-XRD (High Resolution X-ray diffraction) through a Bruker D8 advanced instrument. FTIR (Fourier Transform Infrared) analysis was conducted using the powder of CsNPs, AgNPs, Cs/AgNCs, and Cs/AgNCs/tbn. The ATR method was employed, and the spectra were recorded in the range of 4000 – 500 cm^{-1} using a (PerkinElmer) instrument.

2.4. Antibacterial potential of nanoparticles

The antibacterial activity of plant extract, CsNPs, AgNPs, Cs/AgNCs, and Cs/AgNCs/tbn against *P. aeruginosa* was evaluated using the Kirby-Bauer disk diffusion susceptibility test, following the method described by Bauer (1966). Single bacterial colonies were chosen and incubated overnight in Mueller-Hinton broth (MHB) at a temperature of 37 °C and a speed of 250 rpm. The optical density of the resulting bacterial suspension was determined at a wavelength of 600 nm using a spectrophotometer and then adjusted to a concentration of 1 × 10^6 CFU/mL. Mueller-Hinton Agar (MHA) plates were prepared and subsequently inoculated with the adjusted bacterial suspension. Sterile 6 mm paper discs filled separately with sterile D·H_2O (control), tobramycin, CsNPs, AgNPs, Cs/AgNCs, Cs/AgNCs/tbn with a different concentration (5 to 20 µg/mL) were placed on the MHA plates. The plates were subsequently incubated at 37 °C for 24 h and visually inspected for the zone of inhibition (ZOI) around the discs, indicating the bioactivity of the substance in the discs.

To assess the dose-dependent antibacterial efficiency, a modified MTT assay was conducted following a protocol based on Krishnaraj et al., (2010). Briefly, 100 µL of sterile media was added to each well of a 96-well plate. Starting from the first well of each row, a 200 µg in 100 µL concentration of all the reactants was added, and serial dilutions were performed. Then, 100 µL of bacterial strains were added to all the wells, followed by incubation for 12 h at 37 °C. Control wells were maintained for all the test pathogens without the addition of nanomaterials. Subsequently, a known concentration of MTT solution (5 µL of 0.5 %) was added to all the wells, and the absorbance was measured using an ELISA reader at OD_{595}.

2.4.1. Mode of interaction and ROS generation

To better understand the antibacterial mechanisms of the nanomaterials, the reactants were exposed to interactions with test bacteria. In this process, a 20 mL bacterial culture was subjected to ultrahigh-speed centrifugation at 6000 rpm for 10 min at 4 °C, followed by dispersion in 2 mL of D·H_2O. Subsequently, 1 mL of the dispersed bacterial pellet mixture was combined with AgNPs, CsNPs, Cs/AgNCs, and Cs/AgNCs/tbn at a concentration of 100 µg/mL and allowed to incubate overnight. The resulting interactions were observed using Bio-TEM.

The 2′, 7′-dichlorofluorescein diacetate is used to measure and quantify reactive oxygen species (ROS) in bacteria induced by AgNPs, CsNPs, Cs/AgNCs, and Cs/AgNCs/tbn. Phosphate-buffered saline (PBS) was initially used to treat the bacteria. Subsequently, the cells (1 mL) were exposed to AgNPs, CsNPs, Cs/AgNPs, and Cs/AgNCs/tbn with a concentration of 40 µg/mL and then incubated for 1 h at 37 °C. After

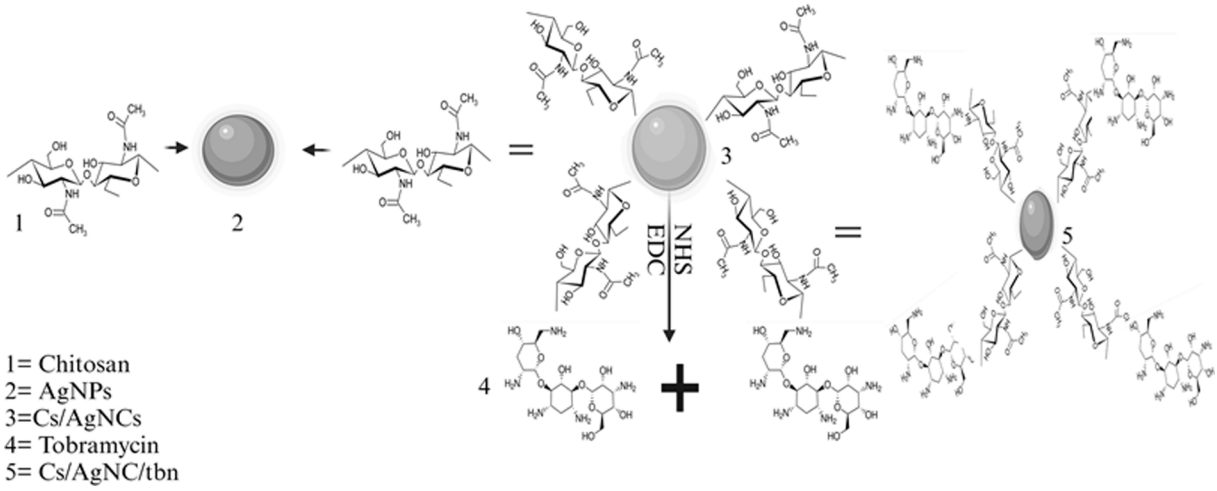

Fig. 1. Describes the formation of Cs/AgNCs/tbn.

washing with PBS, the samples were incubated for 30 min without light with 10 μM DCFDA concentrations. Lastly, CLSM (confocal laser scanning microscopy) images were captured using green fluorescence detectors, with excitation/emission wavelengths set at Ex/Em = 488/521 nm (Zhang et al., 2022).

2.4.2. DNA degradation study

For the DNA degradation study, first, broth cultures of *P. aeruginosa* were treated with AgNPs, CsNPs, Cs/AgNCs, and Cs/AgNCs/tbn, adjusting the final concentration to 40 μg/mL (40 μg of AgNPs, CsNPs, Cs/AgNCs, and Cs/AgNCs/tbn per 1 mL of broth), the cultures were centrifuged at 13,000 rpm for 10 min. In 1 mL of lysis buffer, the pellets were resuspended and centrifuged again for 10 min. Afterward, the pellets were re-suspended in fresh lysis buffer and boiled in a water bath for 30 min. After cooling to room temperature, DNA supernatants were centrifuged for 10 min at 13,000 rpm and were analyzed by gel electrophoresis. To assess DNA damage, DNA samples at a concentration of 500 μg/mL were prepared in D·H_2O and analyzed using UV–Vis spectrophotometry to measure absorbance in the wavelength range of 200 – 300 nm.

2.4.3. Zebrafish (Danio rerio) maintenance and in vitro toxicity study

A zebrafish aquarium is available at the Department of Food Science and Technology at JBNU in South Korea. The aquarium maintains an automatic temperature of 27.5 ± 1 °C and 80 % humidity with a light cycle of 14 h and a dark cycle of 10 h. Fish of both sexes with weights and lengths of 0.3 g and 24 mm, respectively, were used to produce the embryos. The development of the embryos was monitored using a Leica S9D stereomicroscope, and images were captured using the microscope's digital camera. A Fish Embryo Acute Toxicity Test (FET) was conducted using as-synthesized CsNPs, AgNPs, Cs/AgNCs, and Cs/AgNCs/tbn to assess *in vitro* embryotoxicity. The test was performed using embryonic zebrafish (*Danio rerio*) as a model organism, following Test No. 236 of the OECD guidelines (Lammer et al., 2009).

2.4.4. Nanoparticles toxicity assessment

Under the microscope, fertilized eggs collected within 3 h post-fertilization (hpf), were placed in a multi-well plate with 2 mL of (E3) medium water with (NaCl 5 mM) (KCl 0.17 mM) (CaCl 0.33 mM) and ($MgSO_4$ 0.33 mM) used for the embryo (Cassar et al., 2019), and different concentrations of CsNPs, Ag NPs, Cs/AgNCs, and Cs/AgNCs/tbn from 0.19 to 200 μg/mL added in wells, and the plate was incubated at 28.5 °C in the breeding incubator for 96 h. Observations were made at 24, 48, 72, and 96 hpf using a stereomicroscope, and the endpoints, the lack of movement, coagulation, hatching rate, survival of embryos, and heart rate of each embryo were recorded to assess the toxic effects of the nanomaterials. Each experiment was done in triplicate.

3. Results and discussion

3.1. Synthesis of nanomaterials

This study employs the synthesis of CsNPs, AgNPs, and Cs/AgNCs from *Zingiber officinale* rhizome extract, which is reported for its antimicrobial properties (Menon et al., 2019). The biomolecules present in the extract, such as terpenoids, alkaloids, ascorbic acid, oxalic acid, and flavonoids, play a role in stabilizing and reducing the nanoparticles (Fig. 2). (Jahan et al., 2021). These green-synthesized nanoparticles offer a potential alternative to combat antibiotic-resistant bacteria, addressing issues related to low biocompatibility, short-term efficiency, and chemical instability commonly associated with conventional antibiotics.

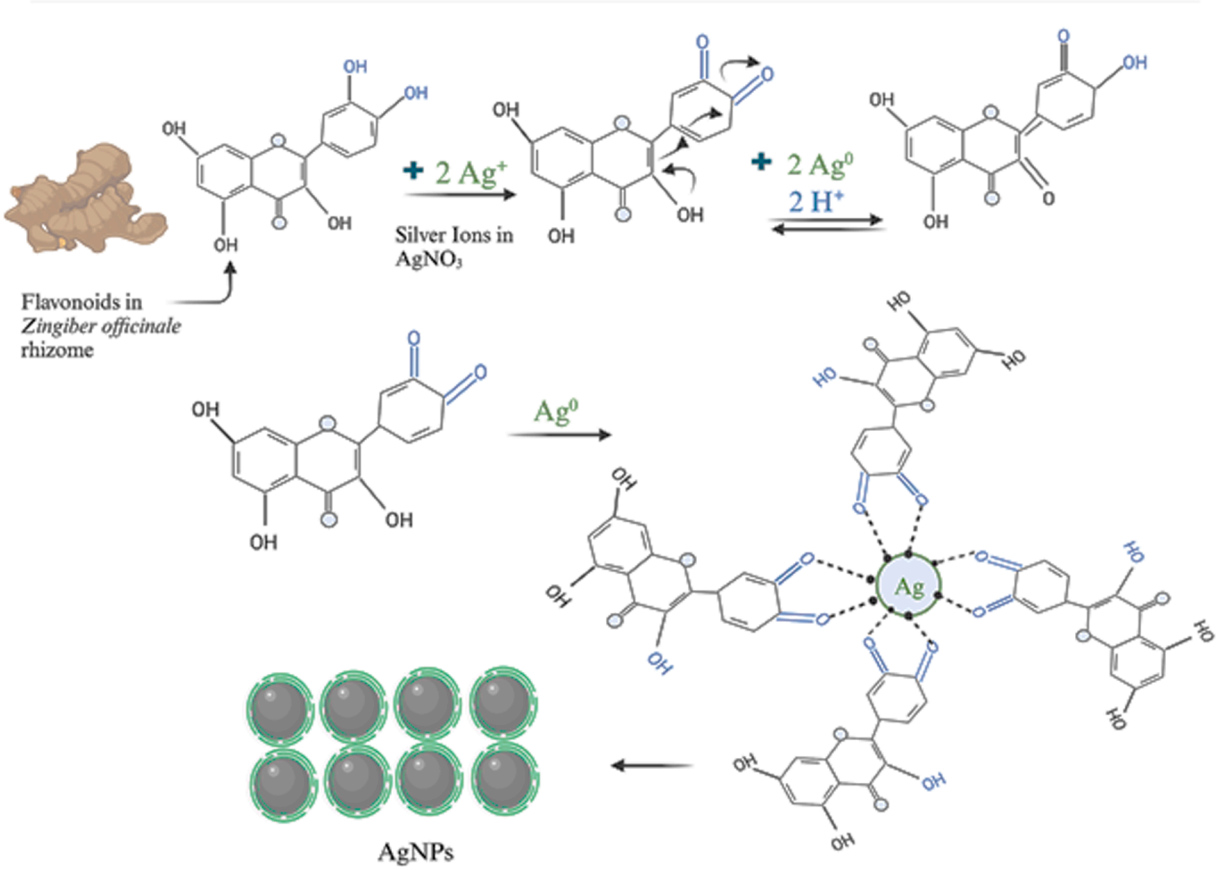

Fig. 2. Schematic Illustration of AgNPs reduction and capping using phytochemicals from *Zingiber officinale* rhizome.

3.2. UV–Vis spectroscopic analysis

UV–Vis spectroscopy was performed to confirm the biosynthesis of nanoparticles. The plant extract, CsNPs, AgNPs, and Cs/AgNCs was scanned at a wavelength ranging from 250 – 600 nm as shown in (Supplementary Fig. S1). The plant extract absorption spectrum showed an absorption peak of 278. This is in agreement with the previous study of Mehata (2021), who reported an absorption peak of ginger extract at 277 nm. The absorption spectra of all nanoparticles ranged between 270 and 322 nm, except for AgNPs, which exhibited absorption between 400 and 500 nm. Each nanoparticle displayed distinct peak values. When 25 mL of ginger extract was mixed with 25 mL of 1 mM $AgNO_3$ solution, the previously transparent solution became a sparkling yellow, indicating the successful synthesis of AgNPs. Confirmation came from the maximum absorbance observed at 432 nm. This synthesis, indicating the presence of AgNPs due to Surface Plasmon Resonance, was further confirmed by the absorption spectrum. For the synthesis of CsNPs, a mixture containing 40 mg of chitosan in 100 mL of 1 % acetic acid was mixed with 25 mL of ginger extract and 8 mL of 0.1 % STPP, revealing a maximum absorbance at 276 nm within the range of 270 – 322 nm. Similar procedures were applied in the synthesis of Cs/AgNCs, differing only in the addition of 100 mL of AgNPs to a solution comprising 100 mL of 40 mg chitosan dissolved in 1 % acetic acid (pH > 6), along with 25 mL of ginger extract and 8 mL of 0.1 % STPP. Remarkably, the Cs/AgNCs exhibited a maximum absorbance at 275 nm, and an absorbance of 1.1893 at 436 nm, confirming the successful synthesis of Cs/AgNCs. These results agree with the previous study of Krishnaraj et al., (2022) who synthesized CsNPs, AgNPs, and Cs/AgNCs using the leaves extract of *Cucurbita pepo*.

3.2.1. Transmission electron microscopy (TEM) and high-resolution X-ray diffraction (HR-XRD) for size and crystallinity analyses

TEM and HR-XRD analyses were performed to characterize and confirm the size, shape, and crystallinity of AgNPs, CsNPs, and Cs/AgNCs. For crystallinity analysis, the diffracted intensities in the whole spectrum of 2θ were recorded between 20° to 90°. The TEM image of AgNPs showed that all the AgNPs are spherical (Fig. 3a) in shape which is very important because shape plays a vital role in the antibacterial activity of nanoparticles. Previous research studies show that AgNPs with spherical shapes are more effective than AgNPs with any other shape. Ciou et al., (2009) argued that spherical AgNPs are more effective because they can effectively interfere with and easily penetrate the bacterial cell membrane. The average diameter of AgNPs was 19 nm making AgNPs the smallest nanoparticles used in this study. The HR-XRD spectrum of AgNPs shows characteristic peaks at 2θ angles of ~ 38.37°, ~44.02°, ~64.74°, and ~ 77.54° which is equivalent to 111, 200, 220, and 311 crystal planes respectively. However, the wider peaks represent the poor crystallinity of AgNPs as shown in Fig. 4a. Fig. 3b showed that the diameter of CsNPs varied between 15–30 nm with an average diameter of 22 nm. The size of nanoparticles significantly affects their antibacterial activity. It has been concluded from previous literature that nanoparticles with a smaller sizes have more significant antibacterial potential than those with larger diameters because of their cell membrane penetration potential (Yin et al., 2020). The HR-XRD spectrum of CsNPs represents characteristic peaks at 2θ angles of ~ 8.79°, ~11.43°, ~29.74°, and ~ 45.69°. These sharp narrow peaks represent the crystalline nature of CsNPs as shown in Fig. 4b. Additional peaks related to *Z. officinale* compounds were also recorded. Fig. 3c. represented the TEM images of Cs/AgNCs showing that almost all the Cs/AgNCs were spherical with increased diameters ranging between 17.09 and 46.64 nm, with 28.61 nm as their average diameter. The average diameter of Cs/AgNCs was larger than that of AgNPs and CsNPs due to their conjugation. A similar study was reported by Butler et al., (2015), who concluded that the size of AgNPs increases upon conjugation. The HR-XRD pattern of Cs/AgNCs displayed the characteristic peaks of both AgNPs and CsNPs as shown in Fig. 4c. Very sharp narrow peaks of Cs/AgNCs at 2θ angle of ~ 8.76°, ~18.98° for CsNPs and at ~ 37.50°, ~44.52°, ~66.01°, and ~ 77.04° for AgNPs which equates to a 111, 200, 220 and 311 crystal peaks (respectively) represent the crystallinity of Cs/AgNCs. The additional peaks observed were due to the presence of secondary metabolites during the synthesis of the nanoparticles.

3.2.2. Field emission scanning electron microscopy (FE-SEM) to study surface morphology

The FE-SEM micrographs demonstrated spherical AgNPs with an average size of 40.3 nm (Fig. 5a). No agglomerates were found, revealing the stability of biosynthesized AgNPs, as they can be seen distinctly. The results presented that biosynthesized AgNPs possessed small grain-like particles, that were gathered to shape crystals with a smooth surface (Bharadwaj et al., 2021). The micrograph of CsNPs (Fig. 5b). showed a dense structure with agglomerated particles. The average size of CsNPs was measured to be 52.5 nm. Scattered particles on thin film were observed for Cs/AgNCs, with an average particle size of 49 nm (Fig. 5c). CsNPs were strongly attached to the surface of AgNPs which following the Chi-AgNPs synthesized by Senthilkumar et al., (2019). Being conjugate, Cs/AgNCs/tbn was found to be densely agglomerated (Fig. 5d). The conjugates were partly spherical with an average size of 66 nm, and similar morphologies were preserved throughout.

3.2.3. Energy dispersive spectroscopy (EDS) analysis

The EDS analysis was used to characterize the elemental composition and chemical analysis of all the nanoparticles. Table 1 represents the weight percentage and maps the distribution of all the elements, especially Carbon (C), Oxygen (O), and Silver (Ag) in AgNPs, CsNPs, Cs/AgNCs, and Cs/AgNCs/tbs. The table shows that the most abundant element in all the samples was Carbon. The spectral analysis of AgNPs revealed a distinctive signal indicating the presence of Ag with a weight

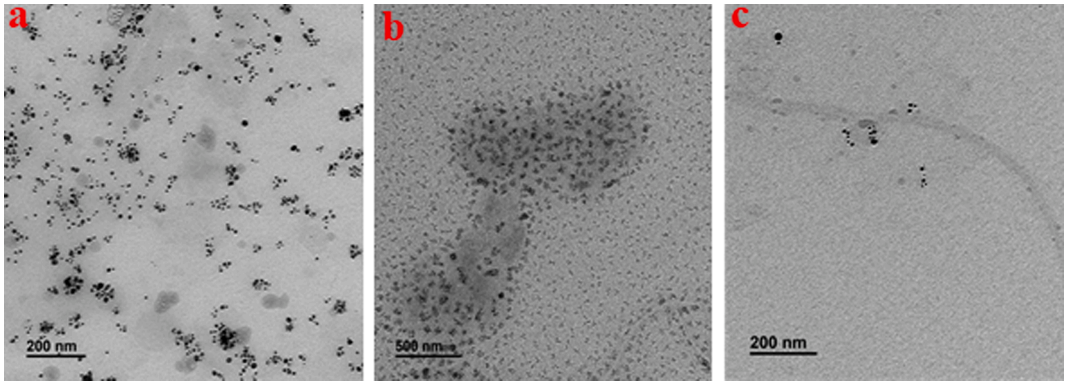

Fig. 3. Transmission Electron Microscopy images of AgNPs (a), CsNPs (b), and Cs/AgNCs (c) for size and shape analysis.

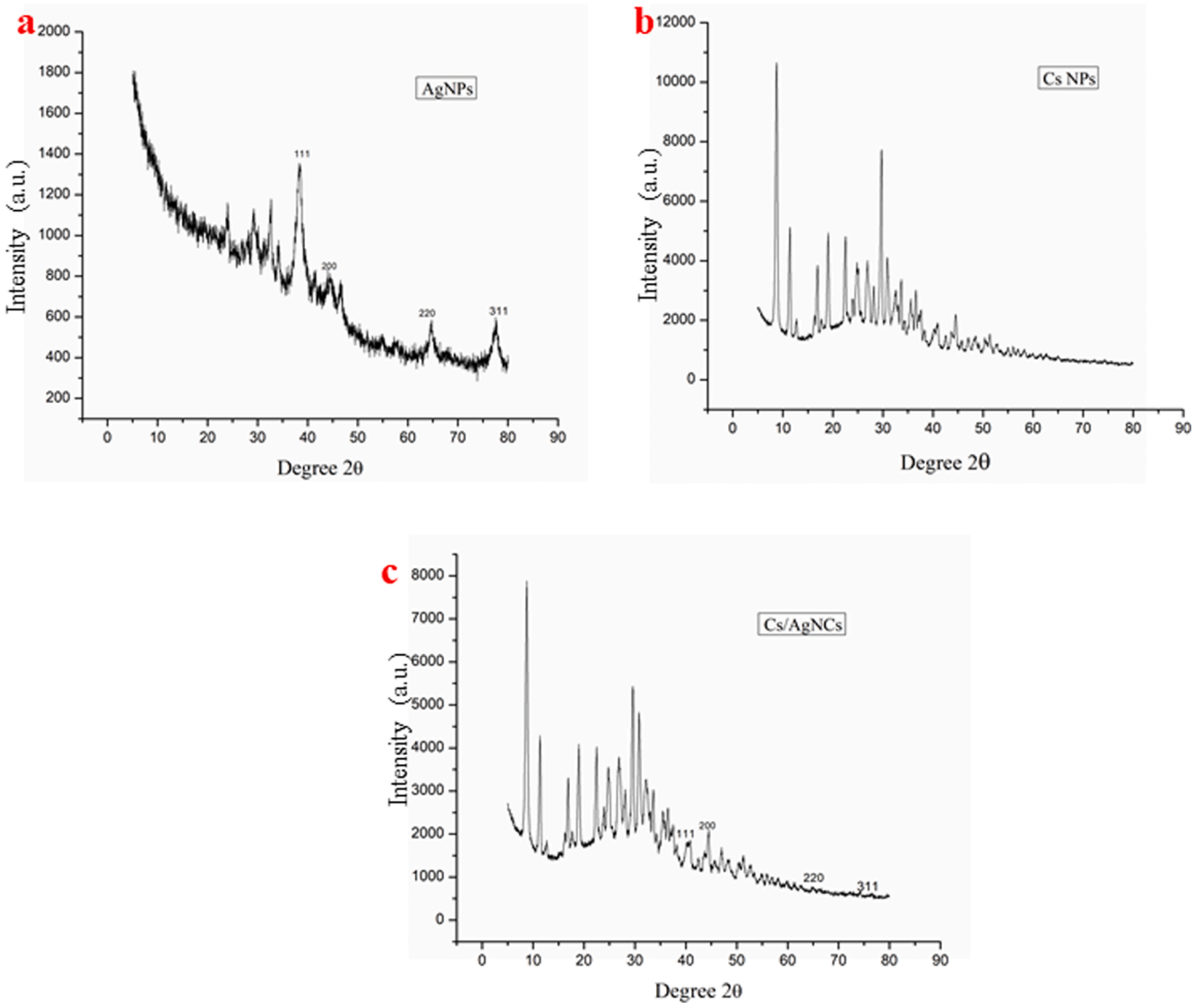

Fig. 4. X-ray diffraction graphs of AgNPs (a), CsNPs (b), and Cs/AgNCs (c) for crystallinity analysis.

percentage of C, O, and Ag at 43.5 %, 19.04 %, and 10.26 % respectively. The high weight percentage of O is due to the supplementation of $AgNO_3$. Some of the weak signals for Mg (0.83 %), Na (1.61 %), P (1.51), S (1.03 %), and Mn (0.68 %) were also observed because the biosynthesis of AgNPs was affected by the interference caused by secondary metabolites (Supplementary Fig. S2a). Similarly, the CsNPs spectrum showed a distinctive signal for chitosan with the weight of C (81.74 %) and (15.65 %) followed by some weak signals of Na, P, and K (2.21 %), (0.29 %), and (0.12 %) respectively (Supplementary Fig. S2b). Our results agree with the study of Krishnaraj et al., (2022) who also reported the high weight of C, and O in both AgNPs and CsNPs but Ag only in AgNPs. The Cs/AgNCs spectrum has demonstrated characteristic signals for both Ag and chitosan with the weight of C (58.96 %), O (23.97 %), and Ag (4.945) (Supplementary Fig. S2c). The presence of various phytochemicals in the leaf extract of *Zingiber officinale* contributed to the biosynthesis. The presence of these phytochemicals is very important for the stability, capping, and bio-reduction of all these nanoparticles (Khan and Ali 2020). The spectrum of Cs/AgNCs/tbs showed the weight percentages of C, O, and Ag as 62.14 %, 22.24 %, and 1.90 %. The weak signal of Mg (0.73 %), Na (0.82 %), P (0.50 %), S (0.43 %), Cl (0.15 %), and K (10.85 %) are also observed (Supplementary Fig. S2d). These elements play a vital role in the synthesis of these nanoparticles giving them antioxidant and antimicrobial capabilities (Khan and Ali 2020). The high abundance and weight percentages of O and Ag are the reason behind the high effectiveness and efficiency of these nanoparticles. For example, our ROS quantification and DNA degradation results showed that AgNPs, Cs/AgNCs, and Cs/AgNCs/tbs with Ag of 10.26 %, 4.94 %, and 1.90 % and high O abundance are more effective than CsNPs with no Ag ions. This indicates that Ag^{+} together with O induces significant oxidative damage to bacterial macromolecules by generating ROS significantly.

3.2.4. FTIR study

The FTIR spectra of samples confirmed the formation of Cs/AgNCs and Cs/AgNCs/tbn by showing the presence of functional groups of compounds of AgNPs, chitosan, and tobramycin that are combined through conjugation (Fig. 6). The FTIR spectrum of Cs/AgNCs showed the absorption of infrared waves by functional groups that were similar to that of AgNPs and CsNPs within the same wavenumber range with slight shifts that indicated the formation of bonds between the compounds after conjugating them with tbn. The absorption bands of AgNPs could be seen at 1669, 1589, 1418, 1269, 1051, 659, and 575 cm^{-1}. These band at 1669 is attributed to C = C (alkene), 1589 to N–H bending (amine), 1418 to C-N stretching (aromatic amine), 1269 to O–H bending (alcohol), 1051 to C-O stretching (primary alcohol), 659 to C-Br stretching, and 575 cm-1 to C-I stretching referring to Halogen

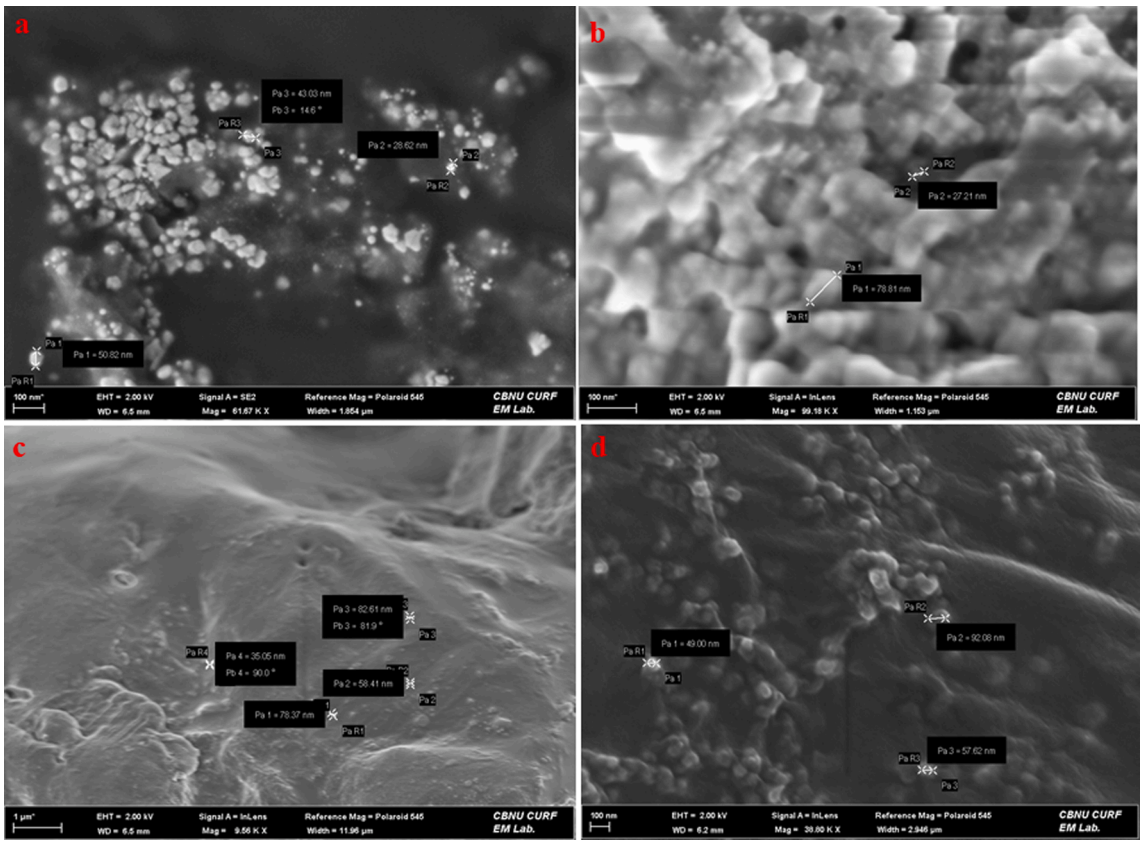

Fig. 5. FE-SEM micrographs representing surface morphology of (a) AgNPs (b) CsNPs (c) Cs/AgNCs (d) Cs/AgNCs/tbn.

Table 1
Weight and atomic distribution of elements of AgNPs, CsNPs, Cs/AgNCs, and Cs/AgNCs/tbn.

Samples	C%	O%	Mg%	Na%	P%	S%	Cl%	K%	Mn%	Ag%
AgNPs	43.59	19.04	0.83	1.61	1.51	1.03	0.74	20.70	0.68	10.26
CsNPs	81.74	15.65	–	2.21	0.29	–	–	0.12	–	–
Cs/AgNCs	58.96	23.97	0.61	1.30	1.09	0.49	0.32	7.22	0.61	4.94
Cs/AgNC/tbn	62.14	22.24	0.73	0.82	0.50	0.43	0.15	10.85	–	1.90

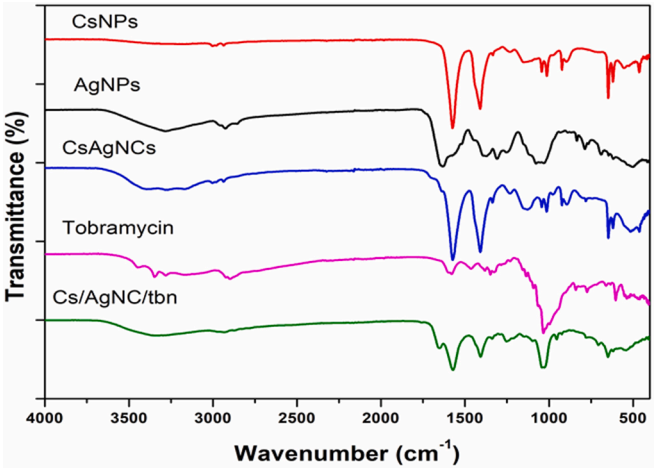

Fig. 6. FTIR spectra of CsNPs, AgNPs, tobramycin, Cs/AgNCs, and Cs/AgNCs/tbn.

compounds. These functional groups were mostly compounds from the ginger extract that had capped silver ions to form silver nanoparticles (Yang et al., 2017). The absorption peaks for CsNPs were observed at 3001, 1573, 1409, 1150, 1043, 1013, 896, 647, 619, and 555 cm^{-1}. The absorption at the given wavenumber corresponded to the presence of C–H stretching (alkene), N–H bending (amine), O–H bending (alcohol), CO stretching (ether), CO-O-CO stretching (anhydride), C-F stretching (fluoro compound), C = C bending (alkene), C-Br stretching, and C-I stretching (halogen compounds), respectively. Tobramycin revealed the presence of N–H stretching (amine), C = H stretching (alkene), C–C stretching (alkene and aldehyde), C–H bending (alcohol), C-O stretching (alcohol), C = C bending (alkene), C–H bending (mono-substitute), O–H bending (alcohol), S-O stretching (sulfonate), C-O stretching, C-Cl stretching and C-Br stretching. These functional groups were identified based on their absorption at 3347, 2898, 1578, 1465, 1381, 1348, 1135, 1092, 840, 773, 659, and 603 cm^{-1}, respectively. The absorption by the same functional groups in the same range (spectra of AgNPs and CsNPs) with little shift was seen in the FTIR spectrum of Cs/AgNCs that showed the combination of AgNPs and CsNPs. The same results were also reported by (Govindan et al., 2012) who reported almost the same functional groups in the same range with little shifts when AgNPs and CsNPs were combined. For example, the bands obtained at 1573 (N–H bending (amine)), 1408 (O–H bending (alcohol)), 1128 (C-O stretching (alcohol)), 780 (C = C bending (alkene)), 619 (C-Br), and 514 cm^{-1}C-I

stretching (halogen compounds) were due to the presence of AgNPs. While the bands at 3270 (C–H stretching (alkyne)), 1336 (S = O stretching (sulfonate)), 1232 (C-O stretching (ether)), 1043 (CO-O-CO stretching), 1013 (C-O stretching (anhydride)), 893 (C-F stretching (fluoro compound)), and 646 cm^{-1} (C–H bending (trisubstitute) were due to the presence of CsNPs. The differences in the wavenumber range might be due to the difference in source for the synthesis of AgNPs. The same assumption was also reported by (Govindan et al., 2012, Ghasemzadeh et al., 2016, Dara et al., 2020) who observed similar functional groups in Cs/AgNCs with somehow little variation in the wavenumber range. Similarly, Cs/AgNCs/tbn is the combination of Cs/AgNCs and tobramycin, so the functional groups detected by the FTIR spectra of tobramycin and Cs/AgNCs could also be seen on the spectrum of Cs/AgNCs/tbn. Almost all the bands observed were the same as that of Cs/AgNCs FTIR spectra except N–H stretching (amine) at 3384, C–C stretching (alkene) at 1670 and 1659, S = O stretching (sulfonate) at 1322, C-O stretching (primary and secondary alcohol) at 1091 and 1059, C = C bending (alkene) at 799, 725 and 705, and C-Br stretching (halogen compounds) at 657. The disappearance of bands similar to tobramycin and composite and the emergence of new bands in the spectrum of conjugation could be due to the occurrence of conjugation. Helal et al., (2014) also observed in their study that some of the original bands of tobramycin disappeared after conjugation and new bands emerged confirming conjugation. Similarly, our FTIR results also align with the previous study of (Armijo et al., 2020), who reported the formation of an amide bond as an indicator of the formation of a conjugate with nanoparticles which here is observed at 1670 cm^{-1}.

3.3. Bacterial cell susceptibility results were determined through disk diffusion and MTT assay

The disk diffusion assay revealed a noticeable trend referring to the increase in the size of the inhibition zone with an increase in the applied volume of each sample (Supplementary Fig. S3). Such a trend has been presented in previous studies showing the dose-dependent activity of antibacterial agents (Zienkiewicz-Strzalka et al., 2019). The largest inhibition zones were observed for Cs/AgNCs/tbn with 20.3 ± 0.33 mm at 20 μL followed by tobramycin (12.6 ± 0.33 mm), Cs/AgNCs (9.66 ± 0.33 mm), and AgNPs (8.33 ± 0.19 mm) (Table 2). Somehow, similar results were obtained by Volova et al., (2018) where silica composite conjugated with antibiotic were found to be more active than the composite conjugated with AgNPs alone. Thus, it's known that antibiotics penetrate the cell membrane and bind irreversibly to their receptors, alter proteins' function, and inhibit the synthesis of bacterial membranes.

The MTT assay used to determine bacterial cell viability with the application of AgNPs, Cs/AgNCs, and Cs/AgNCs/tbn showed significant results that agree with the results of the disk diffusion assay. Importantly, the results might vary with the type of strain being tested. The lowest MIC was recorded for the conjugate of composite with tobramycin i.e., 0.4 μg/mL. Such a low concentration of conjugate was effective because the currently tested strain of bacteria is tobramycin susceptible (inhibited by 1.56 μg/mL of tobramycin). It has been reported in previous literature that MIC of tobramycin could indicate the susceptibility of the bacteria, such as inhibition of the bacterial cell growth at a concentration of ≤ 4 μg/mL shows the specific strain to be susceptible (Armijo et al., 2020). The MIC of AgNPs (12 μg/mL) was lower than that of Cs/AgNCs (25 μg/mL). The antibacterial activity of Cs/AgNCs was most probably due to the presence of AgNPs because CsNPs alone did not show any antibacterial effect (Dara et al., 2020). The nano-silver can disrupt the integrity of the cell membrane, produce oxidative stress, deactivate bacterial proteins by binding to the thiol group, and deactivate metabolic processes such as osmoregulation, electron transport chain, and respiration (Zienkiewicz-Strzalka et al., 2019). The Cs/AgNCs conjugated with tobramycin showed a remarkable antibacterial effect that proves the synergic effect of tobramycin, CsNPs, and AgNPs together. The MIC of Cs/AgNCs/tbn was four times lesser than that of tobramycin alone indicating the reduction of doses by 75 %. A similar synergism was reported in a study where chitosan-AgNPs in combination with different antibiotics were tested against Gram-positive and Gram-negative bacteria (Brasil et al., 2018).

Table 2
Effect of zone of inhibition with varying volumes of samples.

Materials	Zone of inhibition (mm)			
Applied volume	20 μL	15 μL	10 μL	5 μL
Tobramycin	12.6 ± 0.33	11.3 ± 0.33	11 ± 0.57	7.3 ± 0.33
AgNPs	8.33 ± 0.19	8 ± 0.33	8 ± 0.33	–
Cs/AgNC	9.66 ± 0.33	8.33 ± 0.33	7 ± 0.0	–
Cs/AgNC/tbn	20.33 ± 0.33	14.33 ± 0.33	11.33 ± 0.33	10 ± 0.0

3.4. Bio-transmission electron microscopy results determine the mode of action of CsNPs, AgNPs, Cs/AgNCs, and Cs/AgNCs/tbn

To support the antibacterial activity, the interaction of CsNPs, AgNPs, Cs/AgNCs, and Cs/AgNCs/tbn with bacteria was studied through Bio-TEM. Generally, all the tested samples were found to have strong interaction with bacteria which most probably would be the reason for their toxic effect on bacteria. AgNPs adhered to the cell wall of bacteria and then penetrated bacterial cells disrupting the integrity of the cell that ultimately led to bacterial cell death (as shown in Fig. 7a) (Krishnaraj et al., 2015). CsNPs exhibit electrostatic interactions between the amino groups of positively charged glucosamine and the negatively charged bacterial cell membranes. This interaction triggers changes in the permeability of the membrane that results in the efflux of cell components leading to cell death (Chandrasekaran et al., 2020). In Fig. 7b. The interaction of chitosan with the cell wall of *P. aeruginosa* satisfies its proposed antibacterial mechanism. Cs/AgNCs due to their small size and large surface area to volume ratio were shown to interact and penetrate bacterial cell walls (Fig. 7c). Similar results were found in a study where chitosan derivative combined with AgNPs was applied against *E. coli.* When they examined bacterial cells after treatment with Cs/AgNPs, severe detachment of the cell wall from the outer membrane was observed to allow the cytoplasmic content to leave the cell (Huang et al., 2017). In agreement with the results of disk diffusion and MTT assay, Cs/AgNCs/tbn demonstrated a strong bacterial interaction leading to cell disruption (Fig. 7d). The synergic antibacterial effect of AgNPs, CsNPs, and tobramycin enables the conjugate theoretically to target multiple sites of action causing rapid bacterial cell death (Baptista et al., 2018).

3.5. Reactive oxygen species (ROS) quantification

To evaluate the level of oxidative damage caused to bacteria by nanoparticles, ROS was quantified using Confocal Laser Scanning Microscopy (CLSM) after treating the *P. aeruginosa* with plant extract AgNPs, CsNPs, Cs/AgNCs, and Cs/AgNCs/tbn. For this purpose, the level of CHS1, (chilling-sensitive mutant) was determined after treatment and compared to control (untreated bacterial cells), as the level of CHS1 indicates the generation of ROS (Fig. 8). While fluorescence intensity in Fig. 9. showed that all the types of nanoparticles were very effective and resulted in a significant generation of ROS. However, the level of significance varied in the nanoparticles. Cs/AgNCs/tbn was most effective with the highest CHS1 count of 49809, followed by AgNPs (33321). In addition, the results obtained from DNA degradation, MTT, and disc diffusion assays were also confirmed that Cs/AgNCs/tbs were most effective in antibacterial activities, indicating the direct dependence of all types of nanoparticles on their ROS-generating potential. Plant extract and CsNPs generated the lowest levels of ROS with the highest CHS1 counts of 20,217 and 18,650 respectively. Again, this supports the previous assumption because CsNPs caused the least oxidative damage

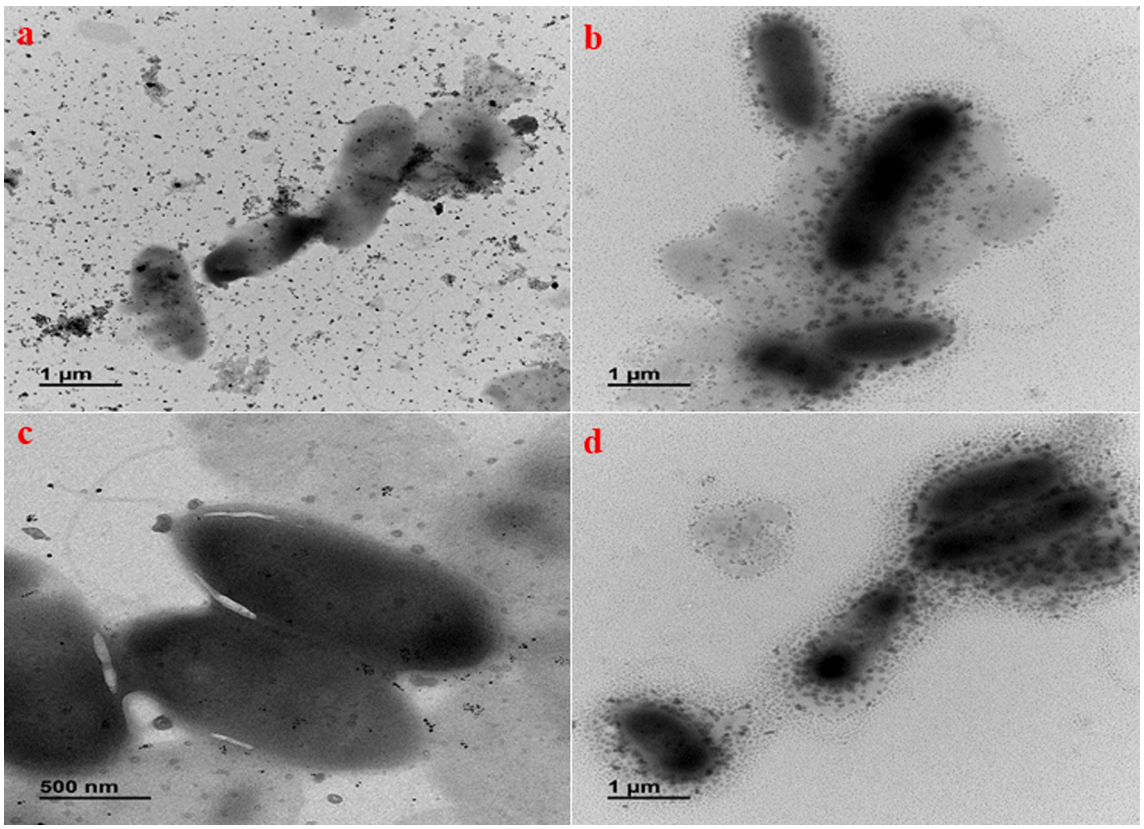

Fig. 7. Bio-TEM micrographs representing biological interaction of a) AgNPs b) CsNPs c) Cs/AgNCs d) Cs/AgNCs/tbn.

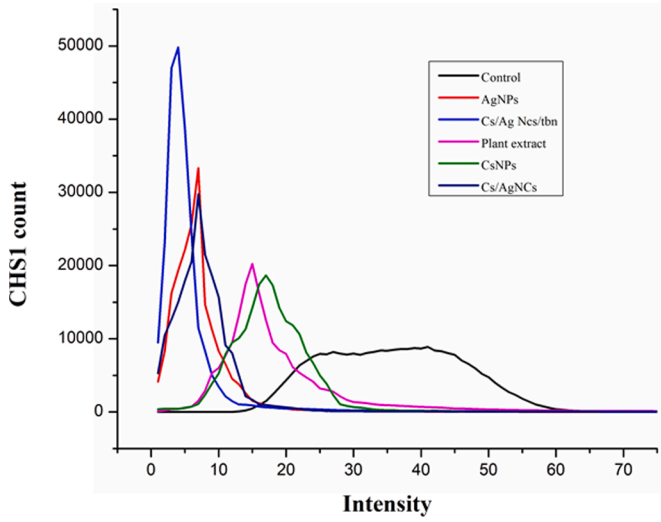

Fig. 8. ROS quantification of *P. aeruginosa* treated with AgNPs, CsNPs, Cs/AgNCs, Cs/AgNCs/tbn.

to the macromolecules of bacteria as shown in DNA degradation, disc diffusion, and MTT assays. The ROS generation potential of Cs/AgNCs (29749) was almost the same as that of AgNPs. A nanoparticle generation of ROS and its antibacterial activity is one of the most researched mechanisms. Also, previous literature suggests that nanoparticles affect bacteria by targeting bacterial lipid and protein membranes by inducing ROS generation leading to bacterial cell death (Gold et al., 2018). Nemčeková et al., (2022) reported that AgNPs-induced oxygen species kill bacteria by altering their DNA by interacting with the charged phosphate backbone of DNA disrupting the electrostatic forces that aid the stability of double helix resulting in the weakened stability of hydrogen bonds between complementary bases. However, Radzig et al., (2013) suggested that ROS targets the bases rather than phosphate groups. When they treated *P. aeruginosa* with AgNPs, they noted that AgNPs generated ROS by inhibiting the enzymes, DNA lesions were formed from the oxidized precursors of DNA. Zhang et al., (2018) argue that the generation of ROS by AgNPs causes oxidative damage to bacteria due to the strong affinity between the positive charge of AgNPs and the negative charge on the peptidoglycan layer of bacterial cell membranes.

3.6. *DNA degradation assay*

The purpose of the assay was to determine whether all the nanoparticles had caused damage to the DNA of *P. aeruginosa*. For this purpose, bacterial cells were treated with plant extract, AgNPs, CsNPs, Cs/AgNCs, and Cs/AgNCs/tbn. The treated cells were scanned at 200–300 nm using a UV–Vis spectrophotometer and their absorbance was compared to the control (untreated bacterial cells). The results showed that all the nanoparticles effectively damaged the bacterial DNA as shown in (Supplementary Fig. S4). However, the level of significance of all the nanoparticles and conjugates varied. The results also showed that Cs/AgNCs/tbn (abs = 0.108 at 280 nm) damaged the DNA of *P. aeruginosa* most significantly. Our results agree with the previous study of Ahmad et al., (2017), who argued that the composition of chitosan and silver nanoparticles significantly damaged bacterial DNA. Interestingly, Cs/AgNCs/tbn was also most effective in generating ROS as shown in (Supplementary Fig. S4). While CsNPs (abs = 0.29) and plant extract (0.325) were the least effective. This also aligns with the results of ROS quantification, as they generated the least ROS. This indicates that the DNA oxidation potential of nanoparticles is directly dependent upon their ROS-generating potential. AgNPs (abs = 0.121) were more effective than Cs/AgNCs (abs = 0.232). This might be due to

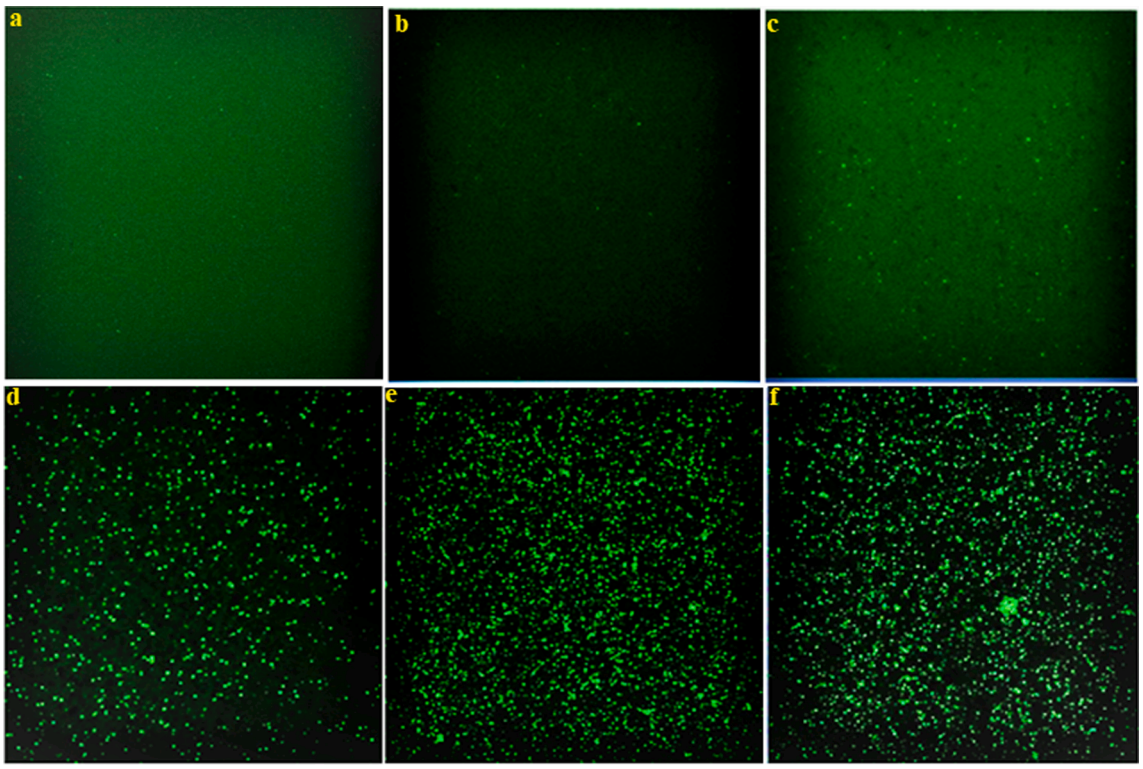

Fig. 9. Fluorescence microscopy images of *P. aeruginosa* treated with plant extract (b), CsNPs (c), Cs/AgNCs (d), AgNPs (e), and CS/AgNCs/tbn (f) compared to Control (a).

an increase in the size of AgNPs when combined with CsNPs because the penetration ability of nanoparticles decreases as their size increases. This assumption agrees with the study of Butler et al., (2015), who reported that the DNA oxidation potential of nanoparticles decreased upon combination with antibiotics or other nanoparticles.

3.7. *In vitro zebra fish embryo toxicity*

In this *in vitro* study, the embryonic toxicity of various concentrations of AgNPs, CsNPs, CS/AgNPs, and Cs/AgNCs/tbn was assessed using zebrafish embryos. The activity of the embryos was monitored from 3 to 96 h, and different parameters were examined to determine if nanoparticles exhibited toxicity towards the fish embryos at a specific concentration (Table 3). The hatching rate of the embryos was evaluated using plant extracts in concentrations ranging between 200 µg/mL to 0.19 µg/mL. Results indicate that the hatching rate of the zebrafish embryos exposed in plant extracts (Fig. 10b), was comparable to the control group (Fig. 10a), from 24 to 96 h. 100 % of the zebrafish embryos hatched successfully, and there was no delay in hatching compared with the control group. The survival rate of the hatched embryos was also similar between the plant extract group and the control. Additionally, the heart rate of zebrafish embryos was assessed after 72 h and compared to the control group. Minor changes were observed in the heart rate of the embryos exposed to plant extract, with values ranging from 120 to 160 beats per minute (bpm), while the control group exhibited a heart rate of approximately 120 to 170 bpm. No structural changes were detected in the zebrafish embryos exposed to the plant extracts.

Table 3
Toxicity assessment of different concentrations of given samples on zebrafish embryos.

Samples	Concentration (µg/mL)	Hatching Rate	Survival Rate	Heart Rate (beats per minute)
Control	N/A	Normal	100 %	120–170 ± 4
Plant extracts	200–0.19 µg/mL	Normal	100 %	120–160 ± 3
AgNPs	200–50 µg/mL	Not Hatched	0 %	–
	25–12.5 µg/mL	Delayed	70 %	101–139 ± 4
	6.25–0.19 µg/mL	Normal	100 %	101–143 ± 3
CsNPs	200–100 µg/mL	Not Hatched	0 %	–
	50 µg/mL	Delayed	80 %	113–154 ± 6
	25–0.19 µg/mL	Normal	100 %	113–157 ± 7
Cs/AgNPs	200–100 µg/mL	Not Hatched	0 %	–
	50–25 µg/mL	Delayed	75 %	108–152 ± 2
	12.5–0.19 µg/mL	Normal	100 %	108–155 ± 6
Cs/AgNC/tbn	200–0.19 µg/mL	Normal	100 %	115–155 ± 4

The toxicity of CsNPs was examined as the same concentration of plant extracts; the CsNPs showed toxicity in higher concentrations ranging from 200 µg/mL to 100 µg/mL (Fig. 10c); no hatching was recorded at higher concentrations. Exposure to 50 µg/mL of CsNPs the hatch rate significantly declined at 48 hpf compared with the control results in a concentration-dependent reduction hatch rate of zebrafish embryos. They were then compared to the control group after being exposed to CsNPs concentration of 25 µg/mL to 0.19 µg/mL for 24 to 72 h of examination. After 72 h, the embryo hatching rate in lower concentrations was closer to the control group. The survival rate at 50 µg/mL was 80 % and from 25 µg/mL to 0.19 µg/mL was 100 % successful and the heart rate in CsNPs compared to the control group increased from 113 to 154 ± 6 bpm. Regarding the structural change in the zebrafish embryo in lower concentration, no significant changes were detected in 96 h of the study. These results are relatable to the results shown by Bhoopathy et al., (2021), where high concentrations of CsNPs (10 – 20 mg/mL) caused malformation of zebrafish embryos. At 20 mg/mL, the mortality rate of zebrafish was shown to be high. Thus, it can be concluded that the toxicity level of CsNPs is dose-dependent and

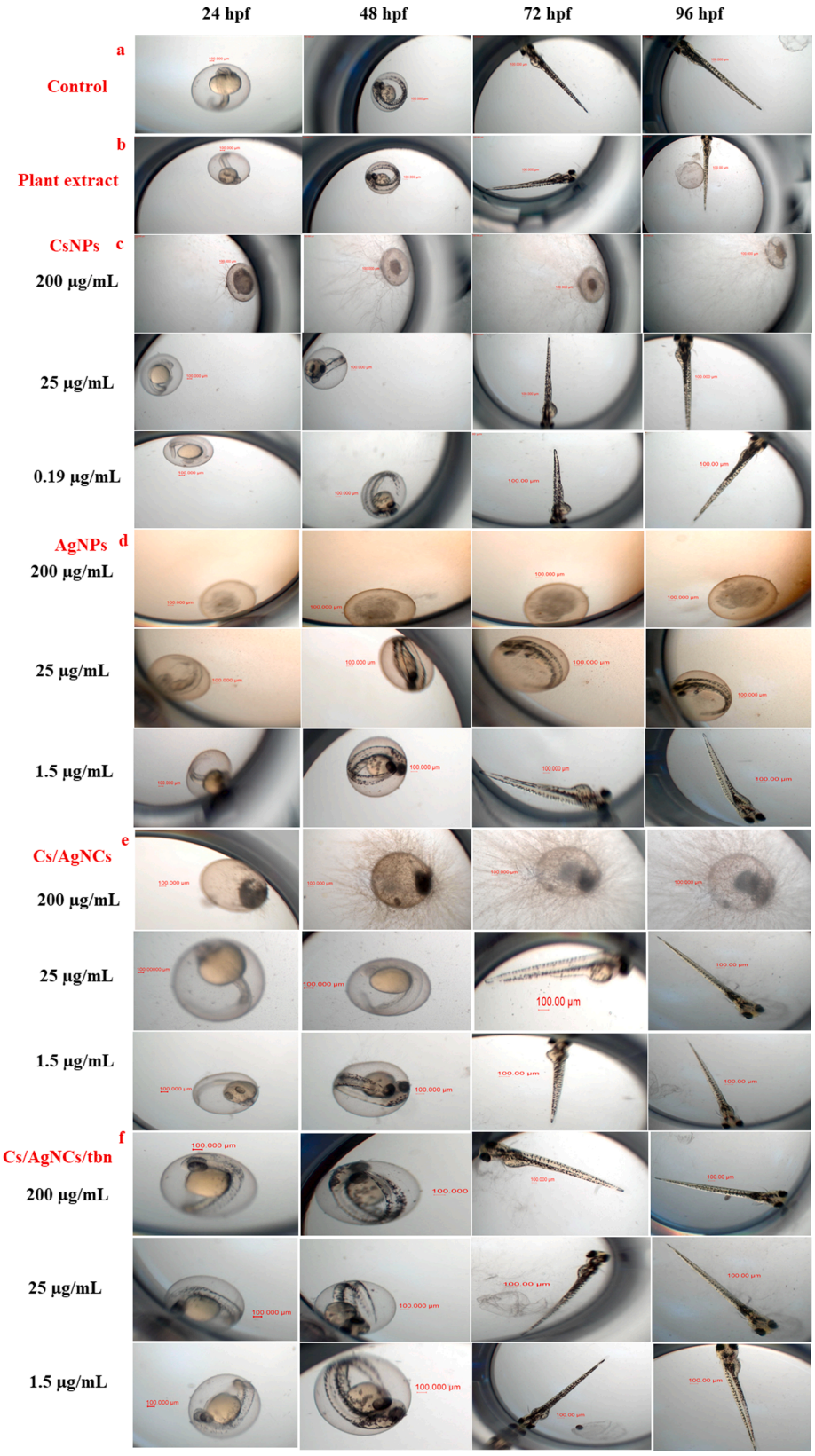

Fig. 10. (a) Control (b) The effect of plant extract on the hatching rate of zebrafish embryos; (c) the effect of various concentrations of CsNPs on the hatching rate, survival rate of zebrafish embryos; (d) the effect of various concentrations of AgNPs on the hatching rate, survival rate of zebrafish embryos; (e) the effect of various concentrations of Cs/AgNPs on the hatching rate, survival rate, of zebrafish embryos; (f) the effect of various concentrations of Cs/AgNCs/tbn on the hatching rate, survival rate, of zebrafish embryos.

increases with increasing concentration.

An analysis of the hatching rate of zebrafish embryos exposed to increasing doses of AgNPs ranging from 200 μg/mL to 50 μg/mL, (Fig. 10d), showed higher toxicity to embryos as observed 0 % hatching rate at 72 hpf. The hatch rate depends on concentration when the concentration decreases to 25–12.5 μg/mL, the embryo hatched delay compared with the control group. The delay in hatching may be due to Ag^{+} released from the dissolution of AgNPs or may be a result of other inhibition processes (Sharma 2020). After 72 h in lower concentrations ranging from 6.25 μg/mL to 0.19 μg/mL AgNPs showed a normal hatching rate. The survival rate of embryos also depends on the concentration of AgNPs. As the concentration of AgNPs increases the number of normally developed zebra fishes decreases, and the mortality rate increases (Krishnaraj et al., 2023). When they were treated with higher doses of AgNPs 200 μg/mL,100 μg/mL, and 50 μg/mL, they showed higher toxicity and they had no survival rate from 24 h to 96 h compared to low doses of AgNPs, the survival rate was increased. It has been reported in previous studies that 142.2 μg/L is critical concentration of AgNPs in adult zebra fishes (Krishnaraj et al., 2016). After this, the heart rate was also calculated and compared to the control, AgNPs significantly decreased the heart rate of embryo zebrafish which was the indicator of toxicity level (Xin et al., 2015). It was recorded after 72 h in 25 μg/mL to 0.019 μg/mL is 101 to 139 ± 4 bpm. AgNPs in 200 μg/mL to 50 μg/mL with higher toxicity demonstrate coagulation, which is not recorded in plant extracts, CsNPs, Cs/AgNPs, and Cs/AgNCs/tbn.

Cs/AgNPs were found to exhibit toxicity at higher concentrations ranging from 200 μg/mL to 100 μg/mL, while no adverse effects were observed at lower concentrations. Exposure to 200 μg/mL and 100 μg/mL of Cs/AgNPs resulted in no hatch rate of zebrafish embryos, particularly at 72 and 96 hpf (Fig. 10e). However, at lower concentrations (50 μg/mL to 25 μg/mL), the embryos exhibited delayed in hatching from 24 to 72 h but showed a hatching rate like the control group after 72 h. The survival rate was 75 % successful in concentrations that range from 50 μg/mL to 25 μg/mL and from 12.5 μg/mL to 0.19 μg/mL, the survival rate increased to 100 %, and the heart rate of the embryos exposed to Cs/AgNPs ranged from 108 to 152 ± 2 bpm, which was comparable to the control group. No significant structural changes were detected in the zebrafish embryos at lower concentrations after 96 h of examination. All the data for Cs/AgNPs shows less toxicity than AgNPs. The possibility for reduced toxicity is the presence of the Cs matrix around Cs/AgNPs (Pérez-Díaz et al., 2016).

The hatching rate of zebrafish embryos was examined using Cs/AgNCs/tbn at concentrations ranging from 200 μg/mL to 0.19 μg/mL (Fig. 10f). A results demonstrated the hatching rate of the embryos exposed to Cs/AgNCs/tbn was comparable to the control group throughout the 24 to 96 h period. The embryos exposed to Cs/AgNCs/tbn showed no delay in hatching referred to the control group, with 100 % of the embryos hatching successfully. The survival rate of the hatched embryos was similar between the Cs/AgNCs/tbn group and the control group. The heart rate of the zebrafish embryos was also assessed after 72 h and compared, to the control group. Minor changes in heart rate were observed in the embryos exposed to the Cs/AgNCs/tbn, ranging from 115 to 155 ± 4 bpm, while the control group exhibited a heart rate of approximately 120 to 170 bpm. No structural changes were detected in the zebrafish embryos exposed to the Cs/AgNCs/tbn. All the data shows that Cs/AgNCs/tbn is less likely to have toxicity toward zebrafish embryos compared to AgNPs, CsNPs, and Cs/AgNPs. Thus, Cs/AgNCs/tbn is the best antibacterial agent with no toxic effect and higher antibacterial activity even at very low concentrations.

4. Conclusions

Finally, our work effectively synthesized AgNPs, CsNPs, and Cs/AgNPs utilizing an environmentally friendly technique that used ginger extract as a reducing agent. The resultant nanomaterials demonstrated favorable optical, thermal, and biological characteristics, making them ideal candidates for biosensing, dye degradation, and surface disinfection. Furthermore, their antibacterial efficacy addressed the critical need for antibiotic-resistance options. UV–Vis spectroscopy, X-ray diffraction (XRD), and Fourier Transform Infrared (FTIR) analyses were used to confirm the structural and chemical characteristics of the synthesized nanoparticles. Cs/AgNPs combined with tobramycin resulted in Cs/AgNCs/tbn, which displayed a substantial increase in antibacterial activity against Gram-negative bacteria, which was related to the development of oxidative DNA damage. This study's findings suggest the possibility of Cs/AgNCs/tbn as a promising nanomedicine for combating bacterial infections. Further investigations should focus on conducting toxicity assessments with longer administration periods and exploring different routes of administration to ensure the safety and effectiveness of this nanomaterial-based therapy. The synthesis of AgNPs and Cs/AgNPs through the green method using ginger extract presents a sustainable and eco-friendly approach, offering a feasible solution for producing nanomaterials with enhanced antibacterial activity. Future research endeavors should explore the potential of these nanomaterials in diverse biomedical applications and optimize their synthesis processes for large-scale production. This study contributes to the advancement of nanotechnology in addressing antibacterial challenges and opens avenues for innovative therapeutic strategies.

Role of the funding source

The funding agency has no role in the preparation of this manuscript; in the design; in the collection; in the writing and in the decision to submit the paper to this journal.

CRediT authorship contribution statement

Shahid Wahab: Conceptualization, Methodology, Investigation, Formal analysis, Writing – original draft. **Haroon Muhammad Ali:** Writing – review & editing. **Maham Khan:** Writing – review & editing. **Tariq Khan:** Writing – review & editing. **Chandran Krishnaraj:** Writing – review & editing, Supervision. **Soon-Il Yun:** Writing – review & editing, Supervision, Project administration, Funding acquisition.

Declaration of competing interest

The authors declare that they have no known competing financial interests or personal relationships that could have appeared to influence the work reported in this paper.

Acknowledgments

This project was supported by the Basic Science Research Program through National Research Foundation of Korea, NRF-2021R1A2C1094316.

Appendix A. Supplementary material

Supplementary data to this article can be found online at https://doi.org/10.1016/j.arabjc.2023.105458.

References

Armijo, L.M., Wawrzyniec, S.J., Kopciuch, M., et al., 2020. Antibacterial activity of iron oxide, iron nitride, and tobramycin conjugated nanoparticles against *Pseudomonas aeruginosa* biofilms. J. Nanobiotechnol. 18, 35. https://doi.org/10.1186/s12951-020-0588-6.

Baptista, P.V., McCusker, M.P., Carvalho, A., et al., 2018. Nano-strategies to fight multidrug resistant bacteria-"A Battle of the Titans". Front. Microbiol. 9, 1441. https://doi.org/10.3389/fmicb.2018.01441.

Bauer, A. J. A. J. C. P., 1966. Antibiotic susceptibility testing by a standardized single diffusion method. 45, 493-496. 10.1093/ajcp/45.4_ts.493.

Bharadwaj, K.K., Rabha, B., Pati, S., et al., 2021. Green synthesis of silver nanoparticles using *Diospyros malabarica* fruit extract and assessments of their antimicrobial,

anticancer and catalytic reduction of 4-Nitrophenol (4-NP). Nanomater.-Basel 11, 1999. https://doi.org/10.3390/nano11081999.
Bhoopathy, S., Inbakandan, D., Thirugnanasambandam, R., et al., 2021. A comparative study on chitosan nanoparticle synthesis methodologies for application in aquaculture through toxicity studies. IET Nanobiotechnol. 15, 418–426. https://doi.org/10.1049/nbt2.12047.
Brasil, M.S.L., Filgueiras, A.L., Campos, M.B., et al., 2018. Synergism in the antibacterial action of ternary mixtures involving silver nanoparticles, chitosan and antibiotics. J. Braz. Chem. Soc. 29, 2026–2033. https://doi.org/10.21577/0103-5053.20180077.
Butler, K.S., Peeler, D.J., Casey, B.J., et al., 2015. Silver nanoparticles: correlating nanoparticle size and cellular uptake with genotoxicity. Mutagenesis 30, 577–591. https://doi.org/10.1093/mutage/gev020.
Cassar, S., Beekhuijzen, M., Beyer, B., et al., 2019. A multi-institutional study benchmarking the zebrafish developmental assay for prediction of embryotoxic plasma concentrations from rat embryo-fetal development studies. Reprod. Toxicol. 86, 33–44. https://doi.org/10.1016/j.reprotox.2019.02.004.
Chandrasekaran, M., Kim, K.D., Chun, S.C., 2020. Antibacterial activity of chitosan nanoparticles: A review. Processes 8, 1173. https://doi.org/10.3390/pr8091173.
Ciou, S.H., Cao, Y.W., Huang, H.C., et al., 2009. SERS enhancement factors studies of silver nanoprism and spherical nanoparticle colloids in the presence of bromide ions. J. Phys. Chem. C 113, 9520–9525. https://doi.org/10.1021/jp809687v.
Dara, P.K., Mahadevan, R., Digita, P.A., et al., 2020. Synthesis and biochemical characterization of silver nanoparticles grafted chitosan (Chi-Ag-NPs): in vitro studies on antioxidant and antibacterial applications. Sn Appl. Sci. 2, 1–12. https://doi.org/10.1007/s42452-020-2261-y.
Ghasemzadeh, H., Sheikhahmadi, M., Nasrollah, F., 2016. Full polysaccharide crosslinked-chitosan and silver nano composites, for use as an antibacterial membrane. Chin. J. Polym. Sci. 34, 949–964. https://doi.org/10.1007/s10118-016-1807-3.
Gold, K., Slay, B., Knackstedt, M., et al., 2018. Antimicrobial activity of metal and metal-oxide based nanoparticles. Adv. Therap. 1, 1700033. https://doi.org/10.1002/adtp.201700033.
Govindan, S., Nivethaa, E.A.K., Saravanan, R., et al., 2012. Synthesis and characterization of chitosan-silver nanocomposite. Appl. Nanosci. 2, 299–303. https://doi.org/10.1007/s13204-012-0109-5.
Helal, H.S., El-Din, T.A.S., Ali, A.E., et al., 2014. Tobramycin-Silver nanocomposite: a new trend of antimicrobials against resistant strains. Pharm. Biol. Sci. 9, 54–61.
Hu, D., Gao, T., Kong, X., et al., 2022. Ginger (Zingiber officinale) extract mediated green synthesis of silver nanoparticles and evaluation of their antioxidant activity and potential catalytic reduction activities with Direct Blue 15 or Direct Orange 26. PLoS One 17, e0271408. https://doi.org/10.1371/journal.pone.0271408.
Huang, X., Bao, X., Liu, Y., et al., 2017. Catechol-functional chitosan/silver nanoparticle composite as a highly effective antibacterial agent with species-specific mechanisms. Sci. Rep.-Uk 7, 1860. https://doi.org/10.1038/s41598-017-02008-4.
Jahan, I., Erci, F., Cakir-Koc, R., et al., 2021. Microwave-irradiated green synthesis of metallic silver and copper nanoparticles using fresh ginger rhizome extract and evaluation of their antibacterial potentials and cytotoxicity. Inorg. Nano-Metal Chem. 51, 722–732. https://doi.org/10.1080/24701556.2020.1808017.
Jelinkova, P., Mazumdar, A., Sur, V.P., et al., 2019. Nanoparticle-drug conjugates treating bacterial infections. J. Control. Release 307, 166–185. https://doi.org/10.1016/j.jconrel.2019.06.013.
Khan, T., Ali, G.S., 2020. Variation in surface properties, metabolic capping, and antibacterial activity of biosynthesized silver nanoparticles: comparison of bio-fabrication potential in phytohormone-regulated cell cultures and naturally grown plants. RSC Adv. 10, 38831–38840. https://doi.org/10.1039/d0ra08419k.
Khan, M., Khan, T., Wahab, S., et al., 2023. Solvent based fractional biosynthesis, phytochemical analysis, and biological activity of silver nanoparticles obtained from the extract of *Salvia moorcroftiana*. PLoS One 18, e0287080. https://doi.org/10.1371/journal.pone.0287080.
Krishnaraj, C., Jagan, E.G., Rajasekar, S., et al., 2010. Synthesis of silver nanoparticles using Acalypha indica leaf extracts and its antibacterial activity against water borne pathogens. Colloids Surf. B Biointerfaces 76, 50–56. https://doi.org/10.1016/j.colsurfb.2009.10.008.
Krishnaraj, C., Harper, S.L., Choe, H.S., et al., 2015. Mechanistic aspects of biologically synthesized silver nanoparticles against food- and water-borne microbes. Bioprocess Biosyst. Eng. 38, 1943–1958. https://doi.org/10.1007/s00449-015-1436-1.
Krishnaraj, C., Harper, S.L., Yun, S.I., 2016. In Vivo toxicological assessment of biologically synthesized silver nanoparticles in adult Zebrafish (Danio rerio). J. Hazard. Mater. 301, 480–491. https://doi.org/10.1016/j.jhazmat.2015.09.022.
Krishnaraj, C., Radhakrishnan, S., Ramachandran, R., et al., 2022. In vitro toxicological assessment and biosensing potential of bioinspired chitosan nanoparticles, selenium nanoparticles, chitosan/selenium nanocomposites, silver nanoparticles and chitosan/silver nanocomposites. Chemosphere 301, 134790. https://doi.org/10.1016/j.chemosphere.2022.134790.
Krishnaraj, C., Radhakrishnan, S., Asmare, M.M., et al., 2023. Green synthesis of Ag and Au NPs decorated rGO nanocomposite for high impedimetric electrochemical sensor as well as enhanced antimicrobial performance against foodborne pathogens. Arab. J. Chem., 105379 https://doi.org/10.1016/j.arabjc.2023.105379.
Kumar, N.V., Murthy, P.S., Manjunatha, J.R., et al., 2014. Synthesis and quorum sensing inhibitory activity of key phenolic compounds of ginger and their derivatives. Food Chem. 159, 451–457. https://doi.org/10.1016/j.foodchem.2014.03.039.
Lammer, E., Carr, G.J., Wendler, K., et al., 2009. Is the fish embryo toxicity test (FET) with the zebrafish (Danio rerio) a potential alternative for the fish acute toxicity test? Comp. Biochem. Physiol. C: Toxicol. Pharmacol. 149, 196–209. https://doi.org/10.1016/j.cbpc.2008.11.006.
Mehata, M.S., 2021. Green route synthesis of silver nanoparticles using plants/ginger extracts with enhanced surface plasmon resonance and degradation of textile dye. Mater. Sci. Eng. B-Adv. 273, 115418 https://doi.org/10.1016/j.mseb.2021.115418.
Menon, S., Devi, K.S.S., Agarwal, H., et al., 2019. Efficacy of biogenic selenium nanoparticles from an extract of ginger towards evaluation on anti-microbial and anti-oxidant activities. Colloid Interface Sci. Commun. 29, 1–8. https://doi.org/10.1016/j.colcom.2018.12.004.
Mori, Y., Ono, T., Miyahira, Y., et al., 2013. Antiviral activity of silver nanoparticle/chitosan composites against H1N1 influenza A virus. Nanoscale Res. Lett. 8, 93. https://doi.org/10.1186/1556-276X-8-93.
Nemčeková, K., Svitková, V., Sochr, J., et al., 2022. Gallic acid-coated silver nanoparticles as perspective drug nanocarriers: Bioanalytical study. Anal. Bioanal. Chem. 414, 5493–5505. https://doi.org/10.1007/s00216-022-03955-2.
Pang, Z., Raudonis, R., Glick, B.R., et al., 2019. Antibiotic resistance in Pseudomonas aeruginosa: mechanisms and alternative therapeutic strategies. Biotechnol. Adv. 37, 177–192. https://doi.org/10.1016/j.biotechadv.2018.11.013.
Pérez-Díaz, M., Alvarado-Gomez, E., Magaña-Aquino, M., et al., 2016. Anti-biofilm activity of chitosan gels formulated with silver nanoparticles and their cytotoxic effect on human fibroblasts. Mater. Sci. Eng. C60, 317–323. https://doi.org/10.1016/j.msec.2015.11.036.
Radzig, M.A., Nadtochenko, V.A., Koksharova, O.A., et al., 2013. Antibacterial effects of silver nanoparticles on gram-negative bacteria: influence on the growth and biofilms formation, mechanisms of action. Colloids Surf. B Biointerfaces 102, 300–306. https://doi.org/10.1016/j.colsurfb.2012.07.039.
Ribeiro, A.I., Dias, A.M., Zille, A., 2022. Synergistic effects between metal nanoparticles and commercial antimicrobial agents: A review. Acs Appl. Nano Mater. 5, 3030–3064. https://doi.org/10.1021/acsanm.1c03891.
Senthilkumar, P., Yaswant, G., Kavitha, S., et al., 2019. Preparation and characterization of hybrid chitosan-silver nanoparticles (Chi-Ag NPs); A potential antibacterial agent. Int. J. Biol. Macromol. 141, 290–298. https://doi.org/10.1016/j.ijbiomac.2019.08.234.
Shao, Y., Wang, Y., Yuan, Y., et al., 2021. A systematic review on antibiotics misuse in livestock and aquaculture and regulation implications in China. Sci. Total Environ. 798, 149205 https://doi.org/10.1016/j.scitotenv.2021.149205.
Sharma, S., 2020. Accessing the developmental toxicity of silver nanoparticles in Zebrafish embryos. Deakin University.
Thi, M.T.T., Wibowo, D., Rehm, B.H.A., 2020. *Pseudomonas aeruginosa* biofilms. Int. J. Mol. Sci. 21, 8671. https://doi.org/10.3390/ijms21228671.
Tyagi, P.K., Gola, D., Tyagi, S., et al., 2020. Synthesis of zinc oxide nanoparticles and its conjugation with antibiotic: Antibacterial and morphological characterization. Environ. Nanotechnol. Monit. Manage. 14, 100391 https://doi.org/10.1016/j.enmm.2020.100391.
Volova, T.G., Shumilova, A.A., Shidlovskiy, I.P., et al., 2018. Antibacterial properties of films of cellulose composites with silver nanoparticles and antibiotics. Polym. Test. 65, 54–68. https://doi.org/10.1016/j.polymertesting.2017.10.023.
Wahab, S., Khan, T., Adil, M., et al., 2021. Mechanistic aspects of plant-based silver nanoparticles against multi-drug resistant bacteria. Heliyon 7, e07448.
Wang, X., Shen, Y., Thakur, K., et al., 2020. Antibacterial activity and mechanism of ginger essential oil against *Escherichia coli* and *Staphylococcus aureus*. Molecules 25, 3955. https://doi.org/10.3390/molecules25173955.
Wang, L.S., Wang, C.Y., Yang, C.H., et al., 2015. Synthesis and anti-fungal effect of silver nanoparticles-chitosan composite particles. Int. J. Nanomed. 10, 2685–2696. https://doi.org/10.2147/IJN.S77410.
Xin, Q., Rotchell, J.M., Cheng, J., et al., 2015. Silver nanoparticles affect the neural development of zebrafish embryos. J. Appl. Toxicol. 35, 1481–1492. https://doi.org/10.1002/jat.3164.
Yang, N., Li, F.Y., Jian, T.C., et al., 2017. Biogenic synthesis of silver nanoparticles using ginger (*Zingiber officinale*) extract and their antibacterial properties against aquatic pathogens. Acta Oceanol. Sin. 36, 95–100. https://doi.org/10.1007/s13131-017-1099-7.
Yang, C.H., Wang, L.S., Chen, S.Y., et al., 2016. Microfluidic assisted synthesis of silver nanoparticle-chitosan composite microparticles for antibacterial applications. Int. J. Pharm. 510, 493–500. https://doi.org/10.1016/j.ijpharm.2016.01.010.
Yin, I.X., Zhang, J., Zhao, I.S., et al., 2020. The antibacterial mechanism of silver nanoparticles and its application in dentistry. Int. J. Nanomed. 15, 2555–2562. https://doi.org/10.2147/IJN.S246764.
Zhang, S., Lu, Q., Zhang, C., et al., 2022. Green synthesis of silver-carbon nanocomposites with extraordinary stability and robust antibacterial activity against bacterial diseases in fish. ACS Appl. Bio Mater. 5, 1064–1072. https://doi.org/10.1021/acsabm.1c01116.
Zhang, L., Wu, L., Si, Y., et al., 2018. Size-dependent cytotoxicity of silver nanoparticles to Azotobacter vinelandii: Growth inhibition, cell injury, oxidative stress and internalization. PLoS One 13, e0209020. https://doi.org/10.1371/journal.pone.0209020.
Zienkiewicz-Strzalka, M., Derylo-Marczewska, A., Skorik, Y.A., et al., 2019. Silver nanoparticles on chitosan/silica nanofibers: characterization and antibacterial activity. Int. J. Mol. Sci. 21, 166. https://doi.org/10.3390/ijms21010166.